Am J Transl Res 2023;15(1):63-81
www.ajtr.org /ISSN:1943-8141/AJTR0144237

Original Article

CircRNA_0263 and circRNA_1507 are dysregulated in a rat model of atrial fibrosis induced by chronic intermittent hypoxia

Xue Liang[1*], Weiding Wang[1*], Yu Liu[2*], Yanhong Liu[3], Manman Wang[4], Wenfeng Shangguan[1], Shuai Miao[1], Tianshu Gu[1], Enzhao Liu[1], Guangping Li[1]

[1]Tianjin Key Laboratory of Ionic-Molecular Function of Cardiovascular Disease, Department of Cardiology, Tianjin Institute of Cardiology, The Second Hospital of Tianjin Medical University, Tianjin 300211, People's Republic of China; [2]Taikang Ningbo Hospital, Ningbo 315100, Zhejiang, People's Republic of China; [3]Heart Center, Tianjin Third Central Hospital, Tianjin 300170, People's Republic of China; [4]Department of Cardiology, Affiliated Hospital of Jining Medical University, Jining 272000, Shandong, People's Republic of China. [*]Co-first authors.

Received May 18, 2022; Accepted November 14, 2022; Epub January 15, 2023; Published January 30, 2023

Abstract: *Aims:* This study aimed to characterize circular RNA (circRNA) profiles associated with atrial fibrosis-related atrial fibrillation (AF) and reveal critical circRNAs for AF. *Methods:* Sprague Dawley rats were randomly divided into control and atrial fibrosis-related AF groups (n = 15 in each group). The rats in the atrial fibrosis-related AF group were induced by chronic intermittent hypoxia (CIH), and then confirmed by electrocardiograms, echocardiography, hematoxylin-eosin staining, Masson staining, immunohistochemistry assays and western blotting. After that, the atrial tissues were sent for circRNA sequencing, and the differentially expressed circRNAs were identified and validated by quantitative real-time polymerase chain reaction (qRT-PCR). Finally, a series of cell experiments were performed to explore the roles of two crucial circRNAs in rat atrial fibroblasts. *Results:* A CIH-induced AF model was successfully established in the rats. After sequencing, five upregulated and 11 downregulated circRNAs were identified in the CIH-induced AF group. These dysregulated circRNAs were primarily associated with "carbohydrate metabolism" and "cardiovascular diseases". Two circRNAs (circRNA_0263 and circRNA_1507) were predicted to regulate target gene expression by interacting with corresponding miRNAs, including rno-miR-29b-5p, rno-miR-29b-3p, rno-miR-496-5p, rno-miR-136-5p, and novel123-mature. Additionally, circRNA_0263 knockdown and circRNA_1507 overexpression inhibited the cell viability of fibroblasts, and downregulated the expression of fibrosis-related proteins. *Conclusion:* A series of circRNAs were identified as dysregulated in an AF rat model, and circRNA_0263 and circRNA_1507 might be crucial for atrial fibrosis-related AF development by competing with several miRNAs.

Keywords: Chronic intermittent hypoxia, atrial fibrillation, atrial fibrosis, circRNA, ceRNA network

Introduction

Atrial fibrillation (AF) is the most common type of cardiac arrhythmia, affecting an increasing number of individuals worldwide. The prevalence of AF is increasing sharply with the aging of the population [1]. Aging and aging-related diseases result in cardiac electrical abnormalities and myocardial remodeling, which increase the occurrence of AF [2]. AF might also accelerate the aging process by causing ischemic or non-ischemic events [3]. Currently, the prevalence of AF is the highest among white populations, with an estimated 7 million individuals diagnosed with AF in Europe and the USA [3, 4]. In Asia, the incidence of AF was reported at 5.38 per 1,000 persons each year, according to a meta-analysis of data from three countries [5]. Multiple factors are associated with an increased risk of AF, including age, arterial hypertension, obesity, diabetes, coronary artery disease, and heart failure. Progressive atrial fibrosis is the primary pathological change reported in AF, associated with disease recurrence and resistance to therapy [6]. However, the molecular mechanisms underlying atrial fibrosis-related AF remain poorly understood.

AF is well known to increase the risk of ischemic stroke, heart failure, and mortality, exacerbat-

ing the overall global health burden. Current treatment options for AF are challenging, especially for AF in older patients. Available therapeutic strategies for AF primarily include antiarrhythmic drug therapy and catheter ablation [7, 8]. Guidelines recommend antiarrhythmic drugs as the initial therapy for symptomatic AF patients. However, recent randomized control trials have suggested catheter cryoballoon ablation as an initial therapy for AF instead of antiarrhythmic drug therapy due to significantly reduced rates of AF recurrence [8, 9]. Clinically, cardiac ultrasound, enhanced computed tomography, positron emission tomography, myocardial contrast echocardiography, enhanced nuclear magnetic field, myocardial biopsy, and other examinations can be used to evaluate the heart structure, pulmonary vein anatomy, and degree of myocardial fibrosis to guide preoperative evaluations and predict prognosis. Recently, a catheter-based ablation of atrial fibrosis, monitored by late gadolinium-enhancement magnetic resonance imaging, has been identified as an effective approach for improving clinical outcome in AF [10]. Investigating the mechanisms that underlie AF will facilitate the exploration of novel approaches to AF prevention and therapy. Obstructive sleep apnea (OSA) has previously been associated with AF [11, 12], and several animal models of AF have been developed, including a rat model of AF induced by chronic intermittent hypoxia (CIH), which appears to closely model AF pathogenesis [13, 14]. However, limited data are available regarding the molecular mechanisms underlying atrial fibrosis in the CIH-induced AF model.

Circular RNAs (circRNAs) are a non-coding RNAs (ncRNAs) that have attracted much attention for the major roles they play in transcriptional and post-transcriptional regulation. Due to their highly conserved sequences and stability in circulation, circRNAs have been extensively investigated in cancers, such as liver, colorectal, and lung cancer [15-17]. Recently, an integrative analysis of circRNA profiles in AF subjects was reported by Hu et al., which identified several dysregulated circRNAs associated with the inflammatory response in AF, including hsa_circ_0007256 and hsa_circ_0003533 [18]. Zhang et al. suggested that circ_0000075 and circ_0082096 might be involved in AF development through the regulation of transforming growth factor-β (TGF-β) signaling pathway [19]. However, the mechanisms through which circRNAs regulate AF have not yet been fully revealed, especially in AF progression.

High-throughput sequencing provides an effective method for the exploration of the pathogenic mechanisms that lead to AF at multiple levels. In this study, we established an atrial fibrosis-related AF rat model induced by CIH and identified differentially expressed circRNAs between the CIH-induced AF group and control group. Functional enrichment analysis was performed, followed by competitive endogenous RNA (ceRNA) network analysis. The differential expression patterns of critical circRNAs were further validated by quantitative real-time polymerase chain reaction (qRT-PCR) assay and their functions were investigated by a series of cell experiments. These results might aid in understanding of the complex mechanisms of atrial fibrosis in the progression of AF.

Materials and methods

Reagents and rats

Primary antibodies were purchased from Abcam, including antibodies against collagen I (COL-1), collagen III (COL-3), connective tissue growth factor (CTGF), TGF-β, matrix metalloproteinase 2 (MMP2), MMP9, α-smooth muscle actin (SMA) and β-actin (details in **Table 1**). Secondary goat anti-rabbit IgG and mouse anti-rabbit IgG antibodies were obtained from Beijing Solarbio Science & Technology Co., Ltd. (Beijing, China).

Thirty healthy male Sprague Dawley (SD) rats (6-8 weeks old), weighing 200-250 g, were purchased from Beijing Vital River Laboratory Animal Technology Co., Ltd. (Beijing, China).

Construction of a CIH-induced rat model

All animal studies were conducted in compliance with the guidelines established by the Animal Administration Committee of Tianjin Medical University (Approval number: TMUaMEC2016012). The rats were randomly divided into a control group and a CIH group, with 15 rats in each group. The rats were allowed free access to normal food and water. The atrial fibrosis-related AF rat model was established by exposure to a CIH environment, using a pre-

Table 1. Primary and secondary antibodies used in western blotting (WB), immunofluorescence (IF) and immunohistochemical (IHC) assay

Primary antibodies	molecular weight	dilution (WB/IHC/IF)	solvent (WB/IHC/IF)
Rabbit anti-Collagen I antibody (ab34710)	130 kDa	1:7500/1:200/-	TBST/PBS/-
Rabbit anti-Collagen III antibody (ab7778)	138 kDa	1:5000/1:200/-	TBST/PBS/-
Rabbit Anti-CTGF (ab6992)	36 kDa	1:4000/1:100/-	TBST/PBS/-
Rabbit anti-TGF β1 (ab170874)	44 kDa	1:1000/1:150/-	TBST/PBS/-
Mouse anti-β-actin (ab32572)	42 kDa	1:5000/-/-	TBST/PBS
Rabbit anti-MMP2 (ab92536)	72 kDa	1:1000/-/-	TBST/-/-
Rabbit anti-MMP9 (ab76003)	92 kDa	1:1000/-/-	TBST/-/-
Mouse anti-α-SMA (ab7817)	42 kDa	1:1000/-/1:500	TBST/-/PBS
Secondary antibodies	-	dilution	solvent
Goat anti-rabbit IgG-HRP (SE00002-1)	-	1:5000	TBST
Mouse anti-rabbit IgG-HRP (SE131)	-	1:5000	TBST

Note: TBST: Tris Buffered Saline Tween; PBS: Phosphate Buffer Saline; HRP: Horseradish Peroxidase; CTGF: Connective Tissue Growth Factor; TGF β1: Transforming Growth Factor beta 1; MMP2: Matrix Metalloproteinase 2; MMP9: Matrix Metalloproteinase 9; α-SMA: α-Smooth Muscle Actin.

viously described protocol [20]. Briefly, the rats in the CIH group were placed in a chamber filled with alternating cycles of nitrogen and oxygen, whereas rats in the control group were raised under normal oxygen conditions. The intermittent hypoxia time was gradually increased from 4 hours every day to 8 hours every day during the first week (from 9:00 AM to 5:00 PM) and then fixed at 8 hours every day. The oxygen concentration was adjusted to 8% from 21% by filling the chamber with nitrogen and was maintained at 8% for 50 s. The oxygen concentration was then increased from 8% to 21% by aerating with oxygen and was maintained for 50 s. Each intermittent hypoxia cycle comprised 300 s, alternating between oxygen concentrations of 8% and 21%.

Data assessment

Intermittent hypoxia exposure lasted for 8 weeks, after which all rats were weighed and anesthetized with ether to perform the echocardiography. Rats were fixed on a platform and assessed by a GE Vivid-7 Doppler ultrasonic machine (General Electric, USA). Interventricular septal thickness (IVS), left ventricular end-diastolic dimension (LVEDD), left ventricular end-systolic dimension (LVESD), left atrial diameter (LAD), and mean pulmonary artery pressure (mPAP) were monitored.

We performed a carotid artery intubation for the blood pressure and ECG monitoring of all rats in both groups. The right common carotid artery was separated from the vagus nerve without damage. Distal ligation was performed with a non-absorbable suture, and a single vascular clamp was fixed on the proximal carotid artery. After a wedge-shaped resection was performed in the middle area, the artery was inserted into a polystyrene catheter (1.5-mm-diameter, injecting heparin sodium) connected to a biological signal acquisition system. ECG data and arterial blood pressure variables were recorded in 10 cardiac cycles, including heart rate, RR interval, PR interval, QRS interval, QT interval, systolic blood pressure, diastolic blood pressure, mean blood pressure, and pulse pressure.

At the end of ECG monitoring, the hearts of rats were collected, weighed, and washed with precooled phosphate-buffered saline three times. The left atrial tissue of five rats in each group was used for hematoxylin-eosin (HE) staining, Masson's trichrome staining, and immunohistochemistry (IHC); all other rat samples were frozen at -80°C for molecular biological analysis.

H&E staining and Masson's trichrome staining

The left atrial tissues were immersed in 4% paraformaldehyde for two weeks. After paraffin-embedding, these tissues were cut into 5-μm sections. The slices were dewaxed in xylene for 10 min, three times, and then moved through a 95%, 80%, and 70% alcohol gradients for gradual dehydration, for 5 min each.

The specimens were then successively stained with hematoxylin for 3 min and eosin for 5 min, followed by reimmersion in alcohol and xylene. Morphological changes were observed under an Olympus CX-21FSI microscope system (Olympus, Japan), and Image-Pro Plus 7.0 software was applied for imaging analysis. Three fields of view were taken from each slide.

Masson's trichrome staining was performed using a kit from Nanjing Jiancheng (Jiangsu, China). Briefly, the left atrial tissues were cut into 5-μm sections. The slides were dewaxed, rehydrated, and immersed in Bouin's solution at 56°C for 15 min. Then, the slides were dyed with Wiegert's hematoxylin, Biebrich scarlet-acid fuchsin, and aniline blue, followed by fixation in 1% acetic acid. Finally, the slides were dehydrated and mounted. Three fields of view were taken from each slide.

Immunohistochemistry (IHC)

The expression levels of fibrosis-related proteins, including COL-1, COL-3, CTGF, and TGF-β1, were detected using IHC. The baked slices were dewaxed with xylene and hydrated with an ethanol gradient (100%-70%). After successively incubating with citrate buffer and 3% H_2O_2 for 30 min, the slides were sealed with blocking solution and incubated with the primary antibodies overnight at 4°C. On the second day, the slides were rinsed and incubated with the corresponding secondary antibody (Zhongshan Jinqiao Biotechnology Company; Beijing, China) for 15 min, followed by 3,3'-diaminobenzidine (DAB) and HE staining. The slides were then examined and photographed (400 ×) using an Olympus BX53 fluorescence microscope (Tokyo, Japan). The DAB staining was analyzed by Image-Pro Plus 7.0 software (Media Cybernetics, Rockville, MD, USA). Three fields of view were taken of each slide. The mean optical density was calculated as the integral optical density/total brown area.

Western blotting

Frozen artery tissue samples were homogenized in radioimmunoprecipitation assay lysis buffer and centrifuged at 12,000 rpm for 15 min. Protein samples (10 μl) were separated by sodium dodecyl sulfate-polyacrylamide gel electrophoresis, transferred onto polyvinylidene difluoride membranes, and incubated with primary antibodies at 4°C overnight (**Table 1**). After washing with Tris-buffered saline containing Tween-20 for 3 times, the membranes were incubated with secondary antibody for 2 h. The signal was visualized using a chemiluminescence kit (Millipore, USA) and exposed using an autoradiographic system.

Identification of the differentially expressed circRNAs

High-throughput sequencing on the three samples of each group was performed by Shanghai OE Biotech Company. Trimmomatic [21] software was used to perform the original data preprocessing, including quality control, read number counts, and summarization. The CircBase database [22] contains numerous circRNA sequences from six species: humans, mice, nematodes, speartail, *Drosophila melanogaster*, and coelacanth. CircRNAs were annotated CIRI software [23]. The prediction results were compared with the CircBase database to obtain known and novel circRNAs.

In addition, circRNA expression was quantified using the reads per million (RPM) method, and the RPM files for circRNAs in each sample were obtained. DESeq software was used to normalize the junction read counts of circRNA in each sample. A negative binomial distribution test was conducted to identify the differentially expressed circRNAs, based on the criteria of $\log_2|\text{fold change}| > 1$ and P-value < 0.05. Cluster analysis was performed for the differentially expressed circRNAs. Gene ontology (GO) and Kyoto Encyclopedia of Genes and Genomes (KEGG) enrichment analyses were performed for the host genes of the differentially expressed circRNAs.

Prediction of circRNA-miRNA interactions

Miranda database was used to predict microRNAs (miRNAs) that interact with the differentially expressed circRNAs. The miRNAs with greater connections to circRNAs were screened using a hypergeometric distribution test. The circRNA-miRNA target interaction network was visualized using R software.

qRT-PCR analysis

The expression levels of critical circRNAs were further validated by qRT-PCR analysis. Total

Table 2. Primers used in real-time PCR

Primer	Sequence (5'-3')	Tm (°C)
GAPDH	F: AGTGCCAGCCTCGTCTCATA	58.0
	R: ACCAGCTTCCCATTCTCAGC	
circRNA_1507|Chr12:41157218_41200958_+	F: TGAAGGAGAGATGCTTCCGA	58.0
	R: GACTTGCCCTTGAGTGTG	
circRNA_0263|Chr1:131552706_131639910_+	F: ACGCCTTCATGTCTGAGTA	58.0
	R: AGCTTTCCTTAAGACCACATTG	

Note: GAPDH: Glyceraldehyde-3-Phosphate Dehydrogenase.

RNA from atrial tissue samples was isolated by TRIzol reagent (Invitrogen, USA) and was reverse transcribed into cDNA by the reverse transcription kit (TIANGEN, Beijing, China). The obtained cDNAs were used for qRT-PCR analysis using a qRT-PCR kit (TransGen Biotech, Beijing, China) on a 7500 RT-PCR System (Thermo, USA). Primers were generated by Beijing BGI Company (Beijing, China), and the primer sequences are shown in **Table 2**. The cDNA levels were analyzed by the $2^{-\Delta\Delta Ct}$ method, and glyceraldehyde 3-phosphate dehydrogenase (GAPDH) was used as an internal control.

Cell culture and treatment

Rat atrial fibroblasts was purchased from Cell Bank of Chinese Academy of Sciences (Shanghai, China) and cultured in complete medium in 37°C with 5% CO_2. Knockdown and overexpression of circRNA_0263 and circ_1507 were achieved by transfection with si-circRNA_0263/circRNA_1507 and oe-circRNA_0263/circRNA_1507 with Lipofectamine 3000 (Thermo Fisher Scientific, Waltham, MA, USA) following the manufacturer's instructions. The effect of knocking down of circRNA_0263 and overexpressing of circRNA_1507 on homologous mRNA were confirmed by qRT-PCR. Afterwards, the cells with different treatment were harvested for Cell Counting Kit-8 (CCK-8, Beyotime Biotechnology, Shanghai, China) in accordance to the protocols. In addition, the expression of α-SMA in the cells with different treatments was measured using immunofluorescence. Western blotting was employed to determine the expression levels of α-SMA, COL-1, COL-3, MMP2 and MMP9 in the cells with different treatments.

Fluorescence in situ hybridization (FISH)

The expression sites of circRNA_263 and circRNA_1507 were identified by FISH as described elsewhere. The rat atrial fibroblasts at 60%-70% confluence were fixed by 4% paraformaldehyde for 10 min. Subsequently, the cells were added with pre-cooled transparent liquid and placed at 4°C for 5 min. Cells were blocked with 200 μl prehybridization solution at 37°C for 30 min. Then, circRNA FISH probe mix and probe hybridization solution were added in cells and incubated at 37°C overnight. At the second day, the cells were hybridized at 42°C, followed by stained with 4',6-diamidino-2-phenylindole for 10 min. The cells were captured using the confocal microscope (Leica, Germany).

Statistical analysis

All experimental data are presented as the mean ± standard deviation. Comparisons between groups were performed by two-tailed *t*-tests in SPSS 19.0 software (SPSS Inc., USA). $P < 0.05$ was considered a significant difference.

Results

Establishment of an AF model induced by CIH

A CIH process was employed to construct a rat model of AF, which was evaluated using electrocardiograms, echocardiography, H&E staining, Masson's Trichrome staining, IHC assays and western blotting. Representative ECG images for control and CIH rats after burst pacing were shown in **Figure 1A**. Cardiac ultrasound analysis of the rat heart showed decreased cardiac systolic function in the CIH group compared with the control group (**Figure 1B**). In addition, after 8 weeks of CIH induction, no significant differences were observed in body weight ($P > 0.05$) or heart mass ($P > 0.05$) between rats in the CIH and control groups (**Table 3**). The basic parameters of mPAP ($P < 0.05$), LAD ($P < 0.001$), left ventricular (LV) internal dimensions ($P < 0.05$), and LV volumes

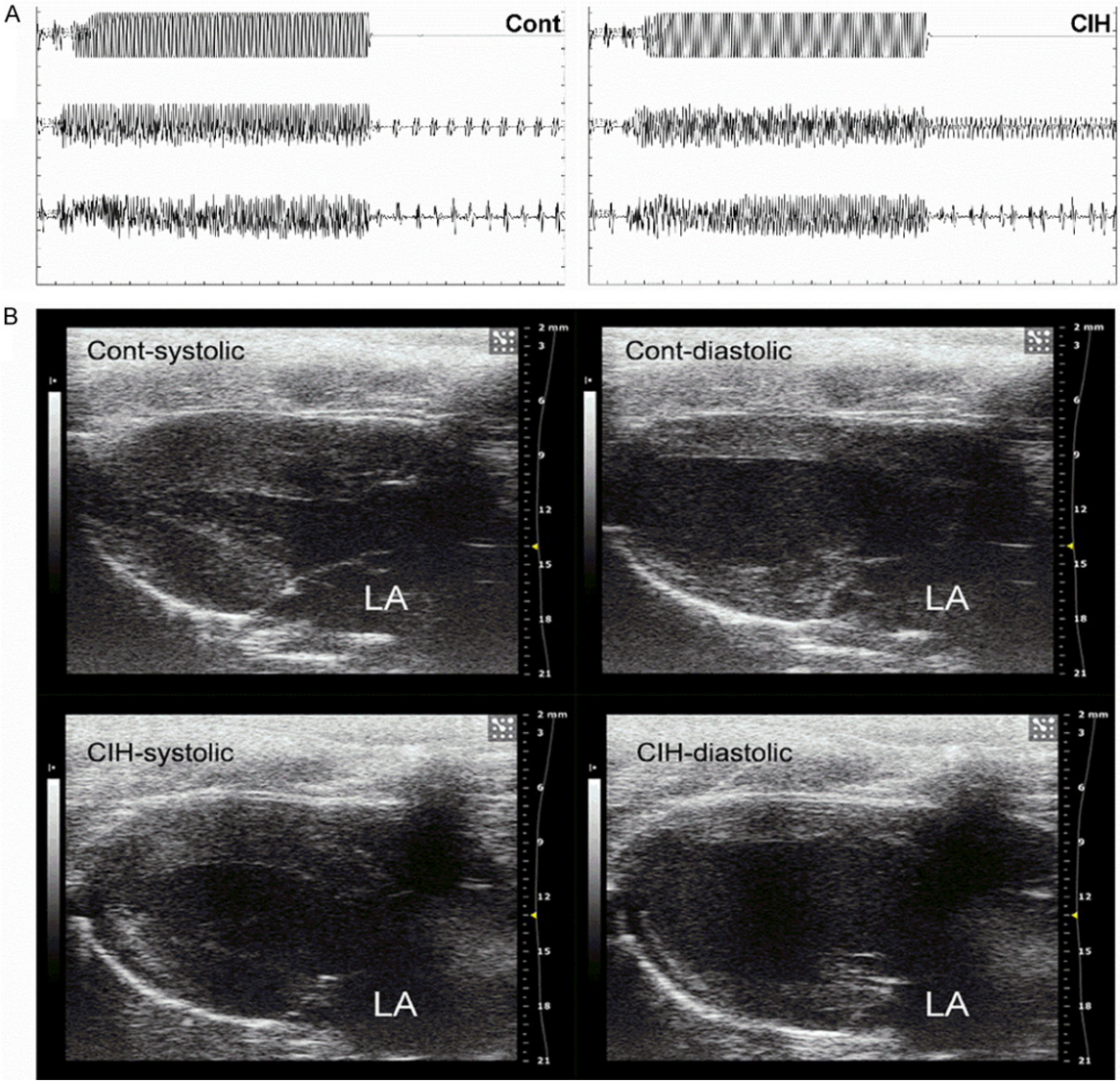

Figure 1. Establishment of an atrial fibrillation (AF) rat model induced by chronic intermittent hypoxia (CIH) using electrocardiograms (ECG) and echocardiography. N = 15. A. Representative electrocardiograms of the control rats and CIH rats. B. Cardiac ultrasonic analysis of rat heart in chronic intermittent hypoxia (CIH, lower) induced rats and normal healthy rats (upper).

($P < 0.05$) were significantly higher in the CIH group than in the control group (**Table 3**). The results for blood pressure and ECG monitoring performed in the two groups of rats are shown in **Table 4**.

H&E staining showed that the atrial muscle cells in CIH rats were larger than those in control rats. Masson's trichrome staining revealed that the atrial tissues of CIH rats presented colored collagen fibers within the interstitial area. The volume fraction of collagen in the atrial tissues exhibited a significant increase (246.47%) in the CIH group compared with that in the control group ($P < 0.001$, **Figure 2**).

Western blotting also revealed that fibrosis-related proteins (COL-1, COL-3, CTGF, and TGF-β) were significantly overexpressed in atrial tissues from the CIH group compared with those from the control group ($P < 0.05$, $P < 0.01$; **Figure 3A**). In the IHC assay, CIH induced the significant deposition of atrial interstitial collagen. The protein expression levels of COL-1, COL-3, CTGF, and TGF-β in the CIH group were significantly upregulated compared to those of the control group ($P < 0.01$, $P < 0.001$; **Figure 3B**). All these results indicated that the CIH-induced AF model was successfully established in the rats.

Table 3. Echocardiography assessment for control group and chronic intermittent hypoxia (CIH) induced-atrial fibrillation rats (n = 15)

Parameter	Control (n = 15)	CIH (n = 15)	*P* value
Body weight (g)	417.75±30.79	401.38±31.27	0.146
Heart weight (g)	1.10±0.12	1.08±0.20	0.724
IVSd, mm	2.40±0.21	2.32±0.30	0.833
IVSs, mm	3.79±0.35	3.36±0.54	0.012
LA, mm	3.55±0.32	4.11±0.26	< 0.001
LVIDd, mm	6.79±0.54	7.05±0.60	0.209
LVIDs, mm	3.46±0.57	4.13±0.81	0.012
LVPWd, mm	2.55±0.30	2.38±0.41	0.201
LVPWs, mm	3.74±0.30	3.48±0.41	0.048
EF, %	78.73±6.90	69.23±14.72	0.026
FS; diameter, %	49.06±6.78	41.32±11.44	0.027
LV Vold, mm^3	240.31±44.17	261.80±49.03	0.203
LV Vols, mm^3	51.57±20.42	79.36±36.60	0.014
mPAP, mmHg	64.00±1.20	65.81±2.42	0.013

IVSd: Interventricular Septal thickness in diastole; IVSs: Interventricular Septal thickness in systole; LA: Left Atrial diameter; LVIDd: Left Ventricular Internal Diameter in diastole; LVIDs: Left Ventricular Internal Diameter in systole; LVPWd: Left Ventricular Posterior Wall thickness in diastole; LVPWs: Left Ventricular Posterior Wall thickness in systole; EF: Ejection Fraction; FS: Fractional Shortening; LV Vold: Left Ventricular Volume in diastole; LV Vols: Left Ventricular Volume in systole; mPAP, mean Pulmonary Artery Pressure; Comparisons between groups were analyzed by two-tailed *t*-tests. *: $P < 0.05$.

Table 4. Blood pressure and ECG monitoring for two groups of rats (n = 15)

	Control (n = 15)	CIH (n = 15)	*P* value
Blood pressure			
Systolic Pressure (mmHg)	153.60±12.01	151.83±22.71	0.814
Diastolic Pressure (mmHg)	119.75±12.10	117.28±18.11	0.699
Mean Pressure (mmHg)	136.06±11.47	134.53±19.41	0.816
Pulse Pressure (mmHg)	33.85±8.07	34.55±5.89	0.811
ECG			
RR Interval (s)	0.16±0.02	0.15±0.02	0.443
Heart Rate (BPM)	330.34±42.05	399.90±55.32	0.046
PR Interval (s)	0.045±0.002	0.047±0.007	0.456
P Duration (s)	0.016±0.001	0.015±0.003	0.748
QRS Interval (s)	0.018±0.003	0.017±0.001	0.507
QT Interval (s)	0.064±0.008	0.079±0.010	0.049
P Amplitude (mV)	0.148±0.031	0.166±0.030	0.184
Q Amplitude (mV)	-0.030±0.022	-0.037±0.022	0.463
R Amplitude (mV)	0.850±0.194	0.852±0.181	0.974
ST Height (mV)	0.041±0.062	0.054±0.039	0.542
T Amplitude (mV)	0.139±0.051	0.183±0.046	0.038

Comparisons between groups were analyzed by two-tailed *t*-tests.

Characteristics of circRNAs in rat atrial tissue

Transcriptomic high-throughput sequencing (including circRNAs, mRNAs, and miRNAs) analysis was performed, and 6,911 circRNAs were identified as being highly enriched in atrial tissue. These circRNAs were derived from 2,875 host genes and consisted of five types: sense-overlapping (6,357; 92%), intronic (37; 1%), intergenic (227; 3%), exonic (217; 3%), and antisense (73; 1%). Among these host genes, 1,509 (53%) host genes produced only 1 circRNA, whereas 54 host genes (2%) produced ten or more circRNAs (**Figure 4**). Most circRNAs were primarily distributed between 200 bp and 1,000 bp in length, and 1,025 circRNAs contained over 2,000 nucleotides (**Figure 4**). The characteristics of these circRNAs are shown in **Figure 4**, including the chromosomal distribution and circRNA lengths.

Screening differentially expressed circRNAs

Using the criteria of $\log_2|\text{fold change}| > 1$ and $P < 0.05$, we identified 16 differentially expressed circRNAs in the CIH group compared with the control group, including 5 upregulated and 11 downregulated circRNAs (**Figure 5A** and **5B**). A volcano plot and an MA plot were used to visualize the differences in gene expression between the two groups (**Figure 5C** and **5D**). Among the dysregulated circRNAs, circRNA_0263 and circRNA_1507 were the most upregulated and most downregulated circRNAs, respectively (**Table 5**).

Functional enrichment analysis

Gene Ontogeny (GO) analysis demonstrated that the host genes

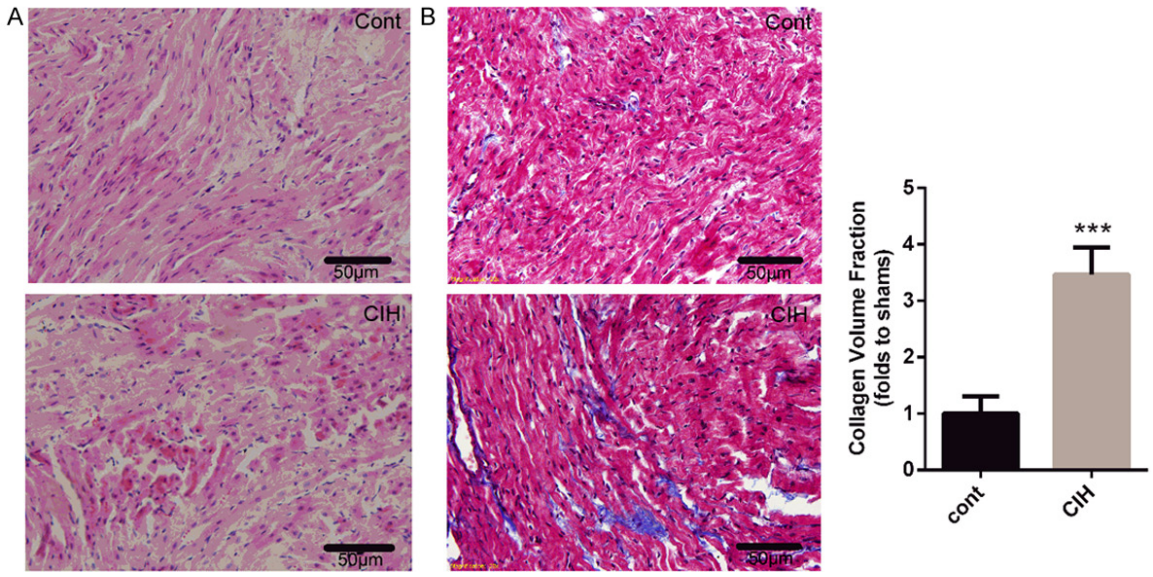

Figure 2. Hematoxylin-eosin staining and Masson staining results of rat atrial tissue in two groups (400×). Comparisons between groups were analyzed by two-tailed *t*-tests. ***, $P < 0.001$.

of the dysregulated circRNAs were primarily associated with the "regulation of biological regulation", "cellular process", "metabolic process", and "response to stimulus". The KEGG pathway enrichment analysis revealed that the host genes of these circRNAs were primarily associated with the pathways "carbohydrate metabolism", "cardiovascular diseases", "immune system", "excretory system", "circulatory system", "glycan biosynthesis and metabolism", "amino acid metabolism", "translation", "substance dependence", "signal transduction", and "transport and catabolism" (**Figure 6**).

Regulatory network involving circRNA-miRNA-mRNA interactions

Next, we constructed ceRNA networks comprised of the two significantly differentially expressed circRNAs, and their associated miRNAs and mRNAs (**Figure 7A**). In these networks, the upregulated circRNA_0263 was predicted to regulate corresponding target genes by interacting with several miRNAs, such as rno-miR-29b-5p/3p, novel33-mature, and novel17-mature. The downregulated circRNA_1507 was predicted to regulate target genes by sponging rno-miR-136-5p, rno-miR-496-3p, rno-miR-337-3p, and novel123_mature. The analysis of the ceRNA network revealed complex and extensive interactions among circRNAs, miRNAs, and mRNAs in atrial fibrosis-related AF.

Validation of critical circRNAs

The expression levels of the two critical circRNAs (circRNA_0263 and circRNA_1507) were further verified by qRT-PCR analysis. Compared to the control group, circRNA_0263 was significantly upregulated in the atrial tissue of CIH-induced AF model rats ($P < 0.05$, **Figure 7B**), whereas circRNA_1507 was significantly downregulated ($P < 0.001$, **Figure 7B**). These results of qRT-PCR analysis were consistent with the high-throughput sequencing results and the bioinformatic prediction, indicating the reliability of our study.

Effects of circRNA_0263 and circRNA_1507 in rat atrial fibroblasts

FISH results showed that circRNA_0263 and circRNA_1507 transcript signals were largely distributed in the cytoplasm of rat atrial fibroblasts (Figure S1). The rat atrial fibroblasts with circRNA_0263/circRNA_1507 overexpression and knockdown were successfully established. Overexpressing or knocking down of these two circRNAs does not affect the expression of their homologous mRNA (Figure S2). CCK-8 results showed that compared with the oe-NC (negative control) group, circRNA_0263 overexpression significantly enhanced the cell viability of fibroblasts ($P < 0.05$); while circRNA_0263 knockdown inhibited the cell viability compared to the si-NC group ($P < 0.05$,

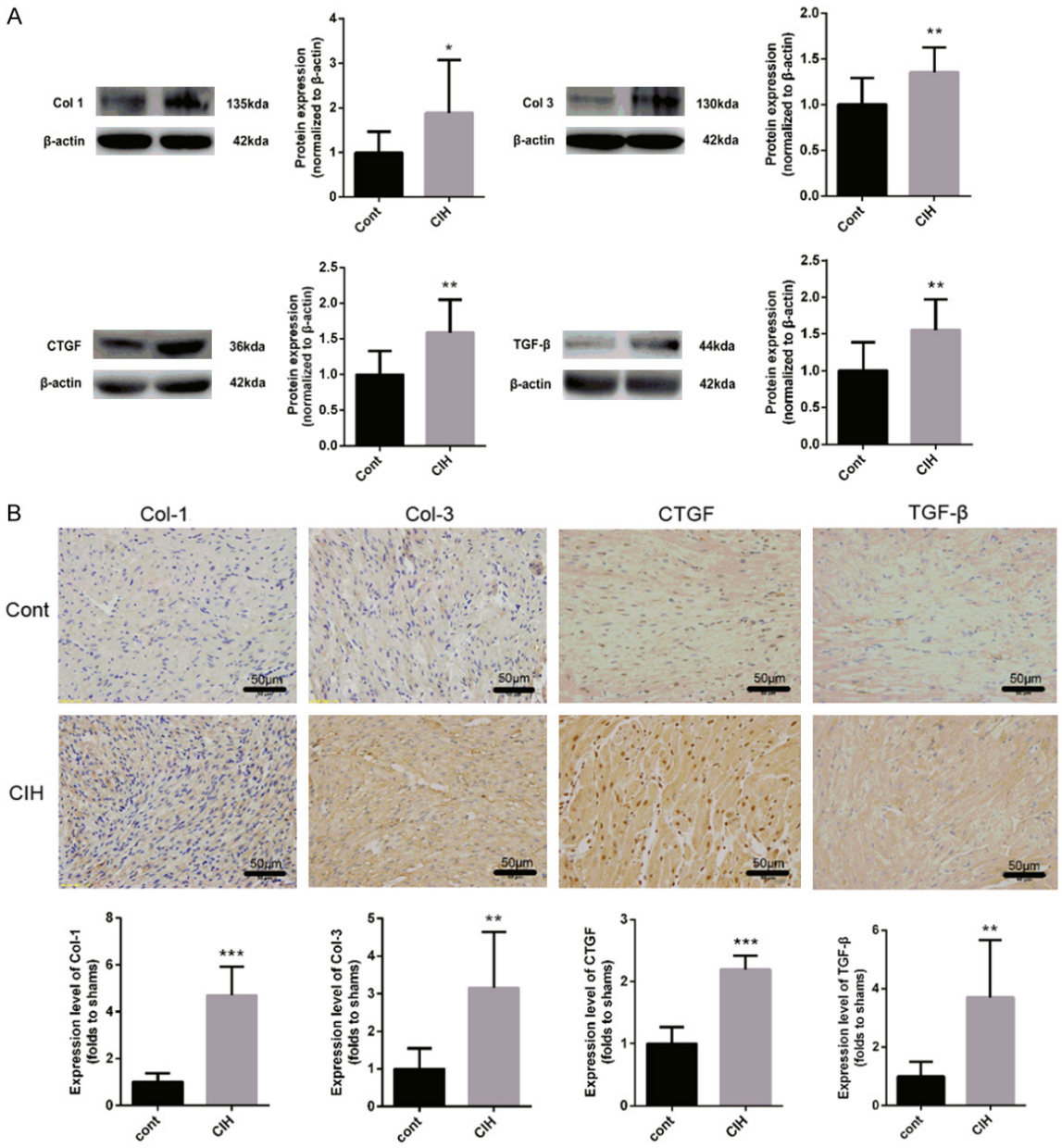

Figure 3. Protein levels of fibrosis biomarkers [collagen I (COL-1), collagen III (COL-3), connective tissue growth factor (CTGF), tumor growth factor-β (TGF-β)] in both groups were detected by using western blotting (A) and immunohistochemistry assay (B). Comparisons between groups were analyzed by two-tailed *t*-tests. $^{**}P < 0.01$, $^{***}P < 0.001$.

Figure 8A). The effects of circRNA_1507 overexpression and knockdown on cell viability in different groups were opposite to those of circRNA_0263 overexpression and knockdown (**Figure 8A**). The immunofluorescence assay showed that the α-SMA expression was significantly increased after circRNA_0263 overexpression and circRNA_1507 knockdown ($P < 0.05$); whereas it was marked reduced when circRNA_0263 was knocked down and circRNA_1507 was overexpressed ($P < 0.05$, **Figure 8B**). In addition, western blotting was used to further determine the protein expression of α-SMA, COL-1, COL-3, MMP2, and MMP9. The expression trend of α-SMA in different groups determined by western blotting was in line with that measured by immunofluorescence assay (**Figure 8C**). For COL-1, COL-3, MMP2 and MMP9, their expression was significantly up-regulated in the circRNA_0263 over-

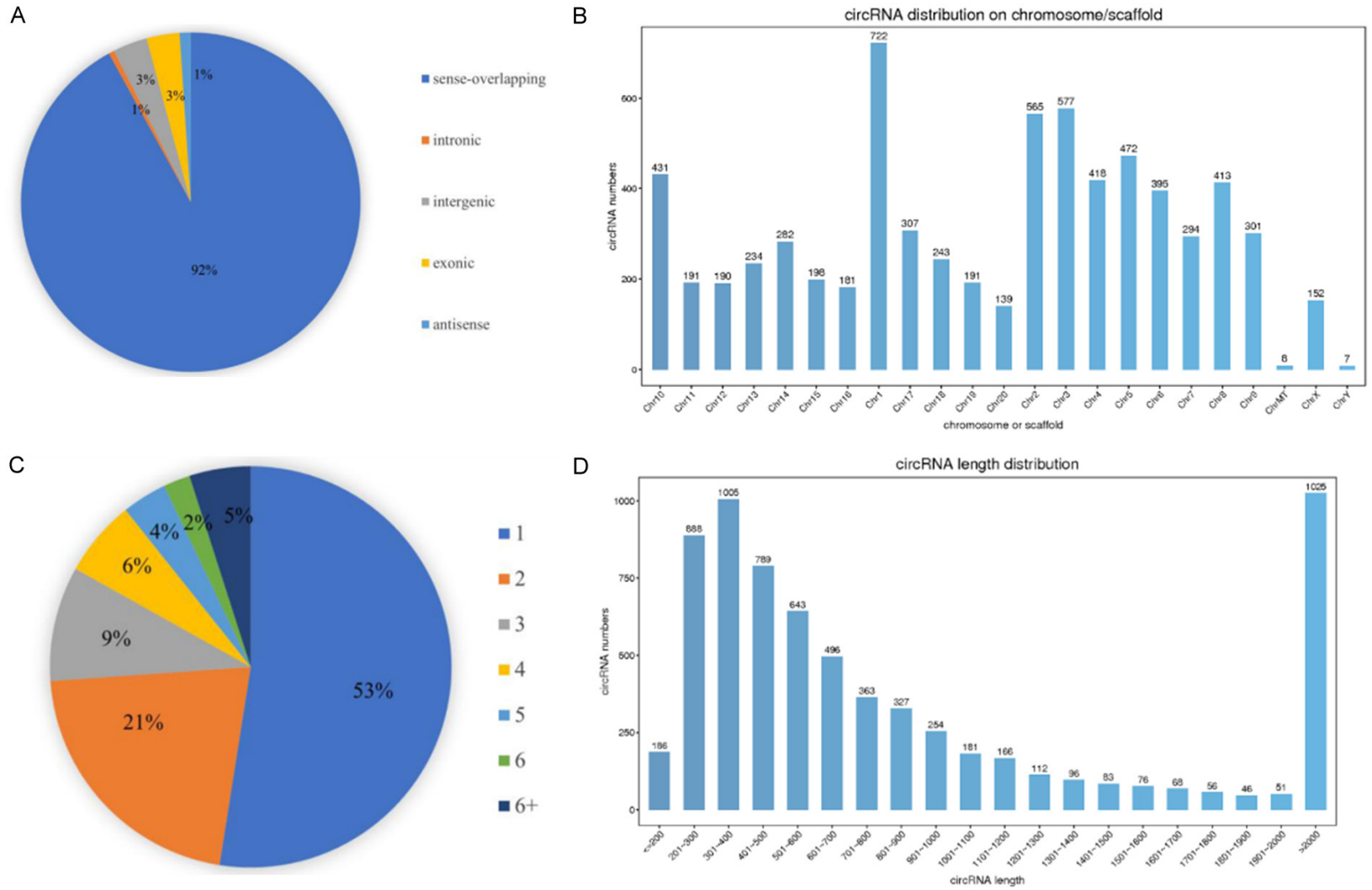

Figure 4. Characteristics of circular RNAs (circRNAs) in rat atrial tissue were visualized, including gene types of circRNAs, distribution on chromosome or scaffold, circRNA numbers produced by host gene, the length of circRNAs.

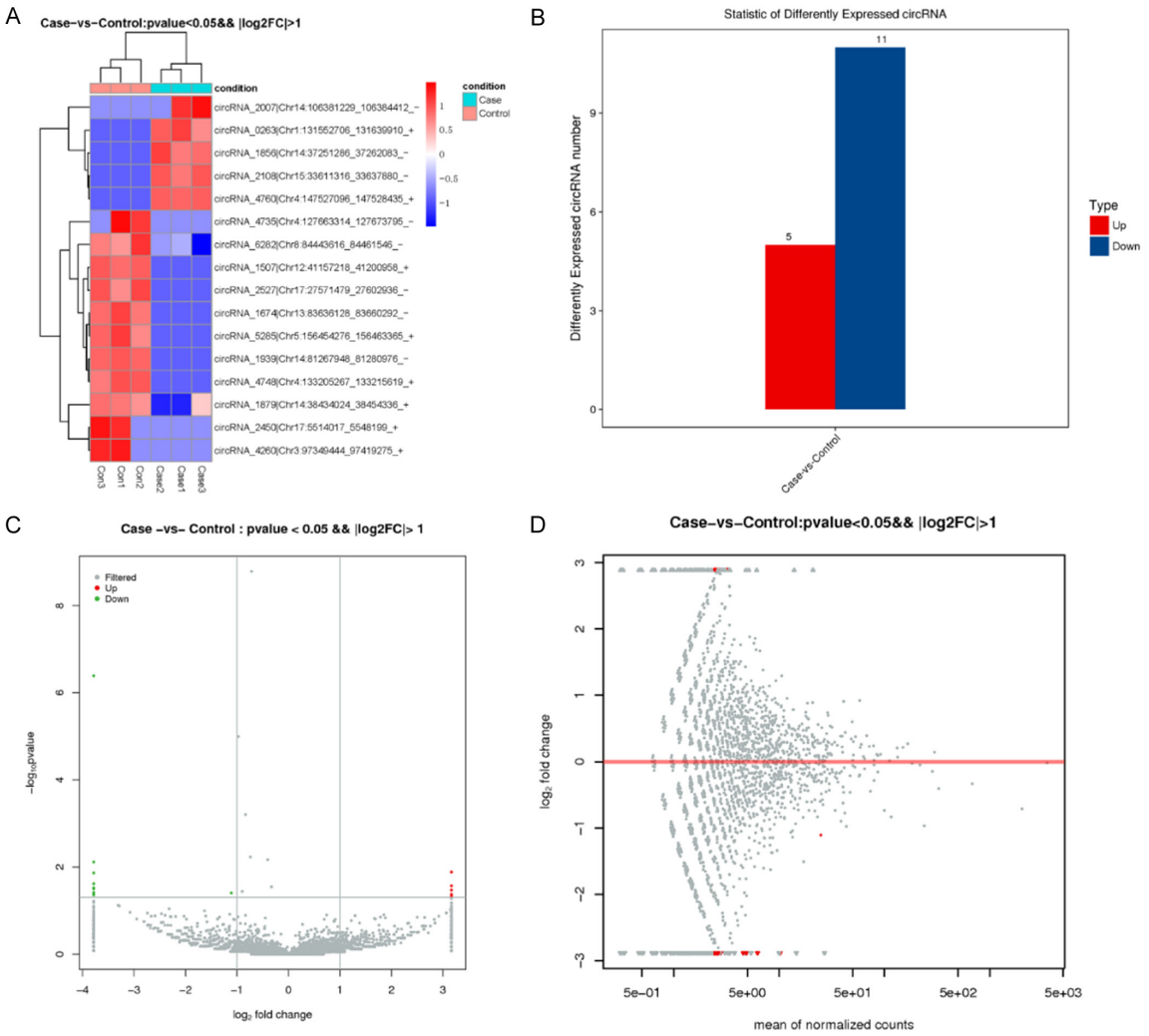

Figure 5. Screening differentially expressed circRNAs from atrial tissue of the CIH group compared to control groups. A, B. Cluster analysis results of 16 differentially expressed circRNAs. Red color indicated upregulated circRNA while blue meant downregulated circRNAs. C, D. Volcano Plot and MA Plot visualized the screening result of differential expressed circRNAs. Gray dots referred to circRNA with non-significant difference. Red and green represented up-regulated and downregulated circRNA.

expression and circRNA_1507 knockdown groups compared with the NC groups ($P < 0.05$), but was markedly down-regulated in the circRNA_0263 knockdown and circRNA_1507 overexpression groups ($P < 0.05$, **Figure 8C**).

Discussion

Atrial fibrillation (AF) is an important clinical disease with increasing impact on public health. Abundant evidence suggests that fibrosis plays a central role in stabilizing reentry drivers of arrhythmias [24, 25]. The content and distribution of fibrous tissue in AF patients are not only related to the pathogenesis of AF, but also related to the risk of complications and treatment failure [6]. Atrial fibrosis is the central pathology of many cardiovascular diseases, including AF. Clinical atrial fibrosis imaging is expected to provide useful information to guide the treatment of AF, and prevention of the development of atrial fibrosis can open up new targets for AF therapy [26, 27]. Therefore, this study established an AF rat model by CIH, and then the atrial tissues were sent for circRNA sequencing. After sequencing, a total of 16 differentially expressed circRNAs were identified, and functional enrichment analysis revealed that the host genes of these dysregulated circRNAs were primarily involved in “biological

Table 5. List of differentially expressed circularRNAs (circRNAs) between the two groups (n = 15)

circRNA	Log_2 Fold change	*P* value	type
circRNA_0263|Chr1:131552706_131639910_+	1.967317783	0.033776083	UP
circRNA_1856|Chr14:37251286_37262083_-	2.188355241	0.027084150	UP
circRNA_2007|Chr14:106381229_106384412_-	1.012044898	0.047278831	UP
circRNA_2108|Chr15:33611316_33637880_-	1.300817414	0.042367506	UP
circRNA_4760|Chr4:147527096_147528435_+	1.621163997	0.013073357	UP
circRNA_1507|Chr12:41157218_41200958_+	-1.520180316	4.08197E-07	DOWN
circRNA_1674|Chr13:83636128_83660292_-	-1.419384032	0.030138812	DOWN
circRNA_1879|Chr14:38434024_38454336_+	-3.782970471	0.013745937	DOWN
circRNA_1939|Chr14:81267948_81280976_-	-1.023897799	0.024104189	DOWN
circRNA_2450|Chr17:5514017_5548199_+	-1.596120571	0.040256919	DOWN
circRNA_2527|Chr17:27571479_27602936_-	-1.834588649	0.031667857	DOWN
circRNA_4260|Chr3:97349444_97419275_+	-1.346870195	0.007670028	DOWN
circRNA_4735|Chr4:127663314_127673795_-	-2.721601859	0.044042436	DOWN
circRNA_4748|Chr4:133205267_133215619_+	-2.171132957	0.030243209	DOWN
circRNA_5285|Chr5:156454276_156463365_+	-1.045020571	0.038325511	DOWN
circRNA_6282|Chr8:84443616_84461546_-	-1.11111	0.039550736	DOWN

regulation", "cellular process", "carbohydrate metabolism", and "cardiovascular diseases". In the ceRNA networks, circRNA_0263 and circRNA_1507 were identified as critical circRNAs involved in the gene regulation of AF through interactions with multiple miRNAs. After that, a series of cell experiments were further performed to verify the roles of circRNA_0263 and circRNA_1507 in rat atrial fibroblasts.

Clinical studies have shown that patients with OSA are vulnerable to the onset of AF [28, 29]. CIH, which is a hallmark of OSA, has been associated with the development of fibrosis in multiple tissues, including the myocardium [20, 30], systemic vasculature [31], liver [32], and lungs [33], and can be employed to construct AF formation. Intermittent hypoxia for a period as short as 4-5 weeks can cause diffuse collagen fiber deposition in rats [33, 34]. In this study, CIH-induced AF was established, and the CIH environment was maintained for eight weeks. Although no significant differences were observed for body weight ($P > 0.05$) or heart mass ($P > 0.05$) between the rats in the CIH and control groups, ECGs and the significantly overexpressed fibrosis-related proteins in CIH group showed the AF model rats were successfully constructed.

Persistent AF leads to electrical remodeling and fibrosis of the atria, which serve as the primary hallmarks of atrial remodeling in patients with AF. Experimental and clinical data suggest that this process involves complex interactions among multiple factors, such as continuous hypoxia, inflammation, oxidative stress, calcium overload, miRNAs, and myofibroblast activation [35, 36]. Here, we examined the protein expression levels of fibrosis-related cytokines in CIH-indued rat atrial tissues. Atrial fibrosis was indicated by the increased expression of COL-1 and COL-3 proteins in both IHC and western blot assays, suggesting the successful establishment of the CIH-induced AF rat model. COL-1 and COL-3 are the major heart collagens and comprise the most common components of the cardiac extracellular matrix (ECM). Alterations in collagen production or degradation have been observed in experimental canine models of AF, as well as in human patients with AF [37, 38]. CTGF is a potent profibrotic factor that promotes cellular adhesion and ECM synthesis. Increased tissue levels of CTGF have been identified in pathological fibrosis states for many organs in heart disease patients, such as the lungs, kidneys, liver, and myocardium [39-41]. TGF-β serves as a major mediator of CTGF signaling and has been reported as upregulated in the atrial tissue of patients with AF [42]. The CIH rat model in our study showed significant upregulation of CTGF and TGF-β, which is in accordance with previous reports [39-42].

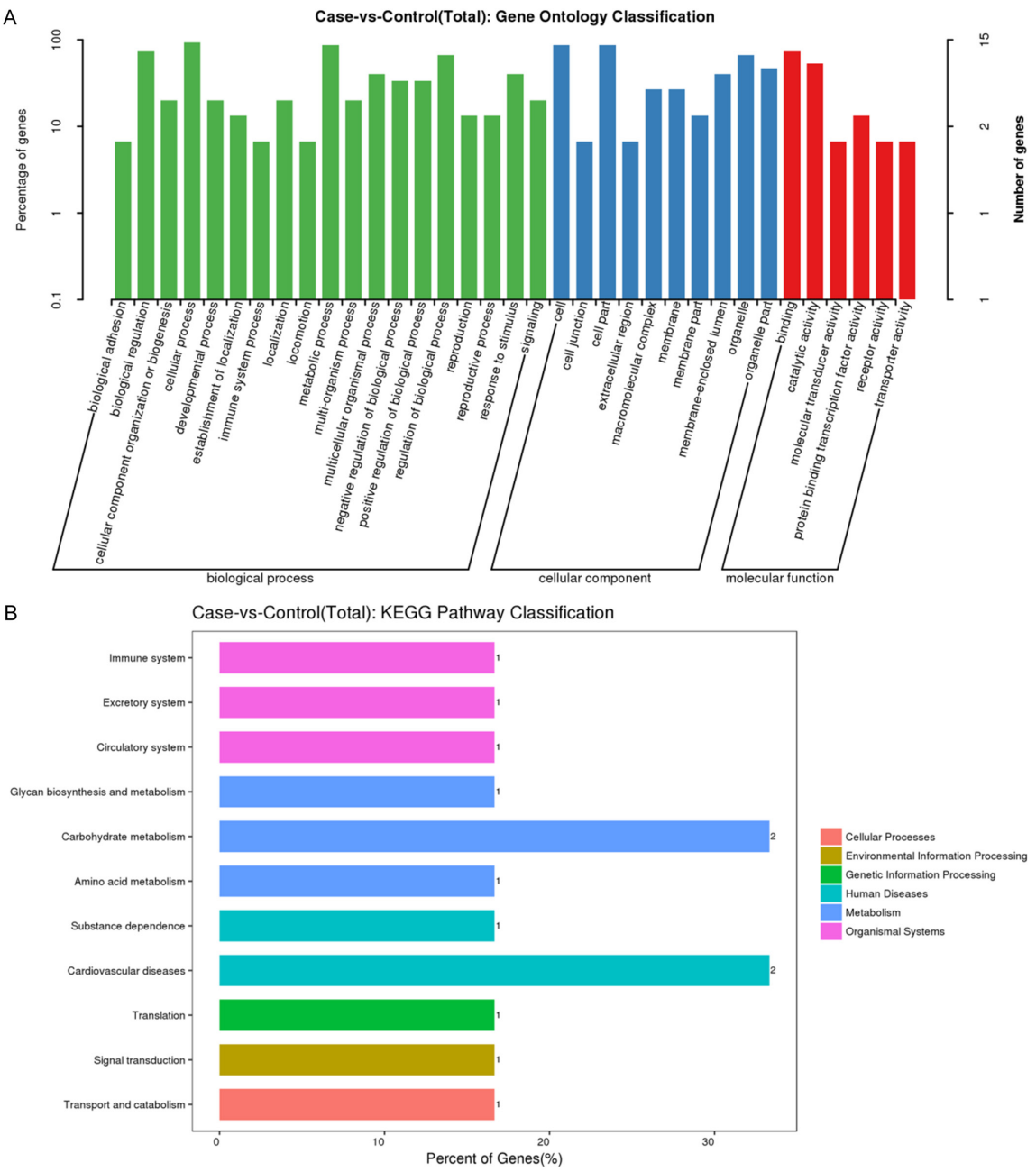

Figure 6. Functional analyses of differentially expressed circRNAs. A. Gene Ontology terms analysis. B. Kyoto Encyclopedia of Genes and Genomes pathways analysis.

CircRNAs are covalently closed RNA molecules that are generated through a process known as back-splicing. Most circRNAs are evolutionarily conserved, and are highly stable [43]. CircRNAs act as ceRNA molecules, involved in several intracellular signaling pathways, and circRNAs can regulate cellular apoptosis and fibrosis in organs. By sponging miRNAs in cells, circRNAs can competitively inhibit the binding of miRNAs with mRNAs, effectively increasing the expression levels of target genes [44]. The roles played by circRNAs were also preliminarily identified during cardiovascular disease development [45]. Based on the ceRNA networks and the qRT-PCR analysis, circRNA_0263 and circRNA_1507 were found to be dysregulated in AF rat atrial tissues. The upregulated circRNA_0263 was predicted to be involved in AF

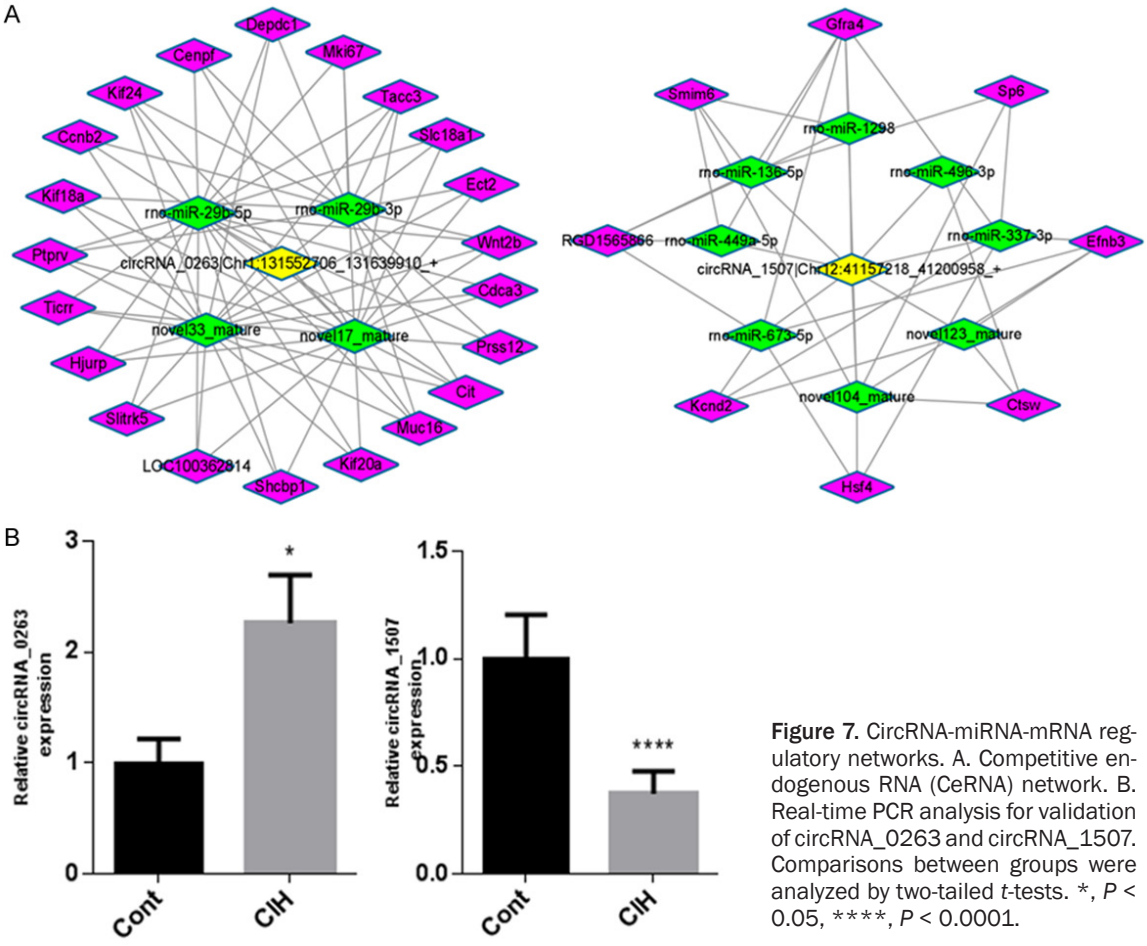

Figure 7. CircRNA-miRNA-mRNA regulatory networks. A. Competitive endogenous RNA (CeRNA) network. B. Real-time PCR analysis for validation of circRNA_0263 and circRNA_1507. Comparisons between groups were analyzed by two-tailed *t*-tests. *, $P < 0.05$, ****, $P < 0.0001$.

progression through interactions with rno-miR-29b-5p/3p, novel33-mature, and novel17-mature. MiR-29 family members play vital roles during fibrosis in many organs through the regulation of fibroblast activation, including lung, cardiac, and hepatic fibrosis [46-48]. MiR-29b is a member of the miR-29 family that was downregulated in a canine atrial fibrosis model, resulting in the increased expression of target ECM genes. TGF-β can induce miR-29b downregulation in atrial fibroblasts, indicating that miR-29b likely regulates the fibrosis processes through the TGF-β signaling pathway [49]. Furthermore, miRNA-29b overexpression alleviated myocardial fibrosis and cardiac dysfunction in post-myocardial infarction rats through the targeting of SH2B3 [50]. In mouse heart tissue, miR-29b prevented angiotensin II-mediated cardiac fibrosis and might represent a therapeutic agent for cardiac fibrosis by targeting the TGF-β/Smad3 pathway [19]. A recent study demonstrated that the miR-29b interaction with Smad3 regulated the expression of migration inhibitory factors, which exhibited an antifibrotic role in cardiac fibrosis [51]. Therefore, we suggest that the circRNA_0263/miR-29b axis could play a crucial role in AF progression. However, the roles played by the circRNAs predicted in our study should be further verified by experimental studies.

The downregulated circRNA_1507 was predicted to regulate the target genes by sponging rno-miR-136-5p, rno-miR-496-3p, rno-miR-337-3p, and novel123_mature. MiR-13-5p is expressed at low levels and acts as a tumor suppressor in many types of cancers [52-54]. MiR-337-3p was demonstrated to promote adipocyte browning by inhibiting TWIST1 in obesity [55] and serves as a tumor suppressor in cancers [56, 57]; however, its role in cardiovascular diseases has not been reported. By constructing the ceRNA network, we demonstrated that these miRNAs might participate in CIH-induced AF by regulating *Smim6*, *Gfra4*, *Sp6,*

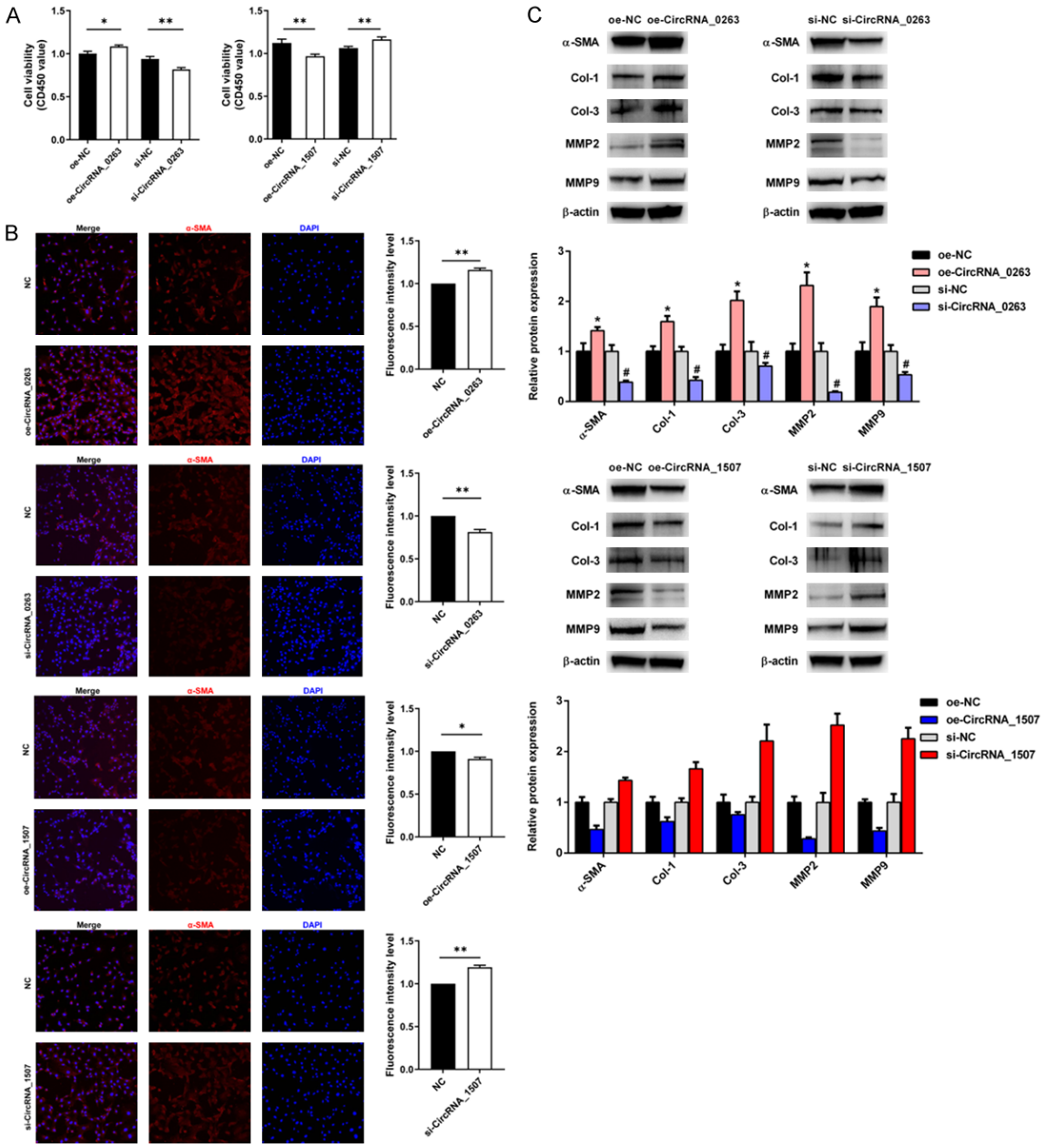

Figure 8. Effects of circRNA_0263 and circRNA_1507 in rat atrial fibroblasts. A. The viability of fibroblasts with circRNA_0263 overexpression/knockdown and circRNA_1507 overexpression/knockdown using Cell Counting Kit-8. B. Expression of α-smooth muscle actin (SMA) in the cells with different treatments by immunofluorescence assay. C. Protein expression levels of α-SMA, COL-1, COL-3, matrix metalloproteinase 2 (MMP2) and MMP9 in the cells with different treatments using western blotting. Comparisons between groups were analyzed by two-tailed *t*-tests. **P* < 0.05, ***P* < 0.01.

and *Efnb3* and could be sponged by circRNA_1507.

In addition, the roles of circRNA_0263 and circRNA_1507 in rat atrial fibroblasts were further investigated. It was found that circRNA_0263 knockdown and circRNA_1507 overexpression could inhibit the cell viability of fibroblasts, and downregulate the expression of α-SMA, COL-1, COL-3, MMP2 and MMP9. COL-1 and COL-3, two major fibrosis-related markers, have been reported as elevated in multiple fibrotic diseases, and play important roles in AF [58]. MMP2 and MMP9 belong to matrix metal-

loproteinase family, and a previous study has found that MMP-2 and MMP-9 levels in blood and atrial tissue had positive connections with AF risk [59]. α-SMA expression is a marker of mature myofibroblasts, and plays an important role in cardiac remodeling [60]. Su et al. showed that miR-133a overexpression could suppress the viability and migration of fibrotic cells and down-regulated the expression of COL-1, COL-3 and α-SMA, thus improving atrial fibrosis-related AF [61]. Another study indicated that cilostazol could have protective effects on rapid atrial pacing-induced atrial remodeling by regulating anti-inflammatory, anti-oxidative stress, MMP2 and MMP9 [62]. Combined with our results, it can be inferred that circRNA_0263 and circRNA_1507 may mediate the growth of atrial fibroblasts via regulating α-SMA, COL-1, COL-3, MMP2 and MMP9, thus playing important roles in AF.

However, this study has some limitations. First, this study was not conducted in aging AF rats; therefore, we were unable to provide a comprehensive description of changes in genes or molecules associated with AF in rats during the aging process. Second, although the differential expression of circRNA_0263 and circRNA_1507 was verified by qRT-PCR, gain-of-function and loss-of-function experiments in this study, further experiments, including dual luciferase reporter assay, RNA binding protein immunoprecipitation or RNA pull-down remain warranted to validated the connection of circRNA_0263 and circRNA_1507 to the miRNAs and mRNAs in the ceRNA network. Additionally, the underlying impacts of circRNA_0263 and circRNA_1507 on cardiomyocytes also need to be further explored.

In conclusion, 16 differentially expressed circRNAs were screened, and were enriched in the carbohydrate metabolism and cardiovascular disease pathways, which play essential roles in promoting AF progression. Additionally, circRNA_0263 and circRNA_1507 were identified as candidate genes involved in the development of AF, which might control target gene expression through interactions with corresponding miRNAs, such as miR-29b-5p/3p, novel33-mature, and rno-miR-136-5p. Our study promotes a better understanding of the circRNA functions in the occurrence and development of fibrosis-related AF.

Acknowledgements

This work was supported by the National Natural Science Foundation of China Youth Science Foundation Project [No. 81700304 and No. 82000313]; The Scientific Research Fund Project of Key Laboratory of Second Hospital of Tianjin Medical University [No. 2019ZDSYS11, No. 2019ZDSYS10, No. 2019ZDSYS02, No. 2019ZDSYS07]; The Research Fund for Central Laboratory of Second Hospital of Tianjin Medical University [No. 2020ydey05]; The Science & Technology Development Fund of Tianjin Education Commission for Higher Education [No. 2020KJ168]; Tianjin Key Medical Discipline (Specialty) Construction Project [TJYXZDXK-029A] and The PhD Research Foundation of Affiliated Hospital of Jining Medical University [No. 2021-BS-005].

Disclosure of conflict of interest

None.

Abbreviations

AF, Atrial Fibrillation; CIH, Chronic Intermittent Hypoxia; circRNAs, circular RNAs; ceRNA, competing endogenous RNAs; COL-1, Collagen I; COL-3, Collagen III; CTGF, Connective Tissue Growth Factor; DAB, 3,3'-Diaminobenzidine; ECG, Echocardiography; ECM, Extracellular Matrix; GAPDH, Glyceraldehyde 3-Phosphate Dehydrogenase; GO, Gene Ontology; HE, Hematoxylin-Eosin; IHC, Immunohistochemistry; IVS, Interventricular Septal Thickness; KEGG, Kyoto Encyclopedia of Genes and Genomes; LAD, Left Atrial Diameter; $\log_2$ FC, $\log_2$ Fold Change; LVEDD, Left Ventricular End-Diastolic Dimension; LVESD, Left Ventricular End-Systolic Dimension; miRNAs, microRNAs; mPAP, mean Pulmonary Artery Pressure; ncRNA, non-coding RNA; OSA, Obstructive Sleep Apnea; qRT-PCR, quantitative Real-Time Polymerase Chain Reaction; RPM, Reads Per Million; SD, Sprague Dawley; TGF-β, Transforming Growth Factor-β.

Address correspondence to: Guangping Li and Enzhao Liu, Tianjin Key Laboratory of Ionic-Molecular Function of Cardiovascular Disease, Department of Cardiology, Tianjin Institute of Cardiology, The Second Hospital of Tianjin Medical University, No. 23, Pingjiang Road, Hexi District, Tianjin 300211, People's Republic of China. E-mail: tic_tjcardiol@126.com (GPL); liu_ezh@126.com (EZL)

References

[1] Ravassa S, Ballesteros G and Díez J. Aging and atrial fibrillation: a matter of fibrosis. Aging (Albany NY) 2019; 11: 9965-9966.

[2] Lin YK, Chen YA, Lee TI, Chen YC, Chen SA and Chen YJ. Aging modulates the substrate and triggers remodeling in atrial fibrillation. Circ J 2018; 82: 1237-1244.

[3] Kallistratos MS, Poulimenos LE and Manolis AJ. Atrial fibrillation and arterial hypertension. Pharmacol Res 2018; 128: 322-326.

[4] Go AS, Hylek EM, Phillips KA, Chang Y, Henault LE, Selby JV and Singer DE. Prevalence of diagnosed atrial fibrillation in adults: national implications for rhythm management and stroke prevention: the AnTicoagulation and Risk Factors in Atrial Fibrillation (ATRIA) Study. JAMA 2001; 285: 2370-2375.

[5] Bai Y, Wang YL, Shantsila A and Lip GYH. The global burden of atrial fibrillation and stroke: a systematic review of the clinical epidemiology of atrial fibrillation in Asia. Chest 2017; 152: 810-820.

[6] Nattel S. Molecular and cellular mechanisms of atrial fibrosis in atrial fibrillation. JACC Clin Electrophysiol 2017; 3: 425-435.

[7] Baher A and Marrouche NF. Management of atrial fibrillation in patients with heart failure: time to implement ablation control. Curr Cardiol Rep 2019; 21: 10.

[8] Wazni OM, Dandamudi G, Sood N, Hoyt R, Tyler J, Durrani S, Niebauer M, Makati K, Halperin B, Gauri A, Morales G, Shao M, Cerkvenik J, Kaplon RE and Nissen SE; STOP AF First Trial Investigators. Cryoballoon ablation as initial therapy for atrial fibrillation. N Engl J Med 2021; 384: 316-324.

[9] Andrade JG, Wells GA, Deyell MW, Bennett M, Essebag V, Champagne J, Roux JF, Yung D, Skanes A, Khaykin Y, Morillo C, Jolly U, Novak P, Lockwood E, Amit G, Angaran P, Sapp J, Wardell S, Lauck S, Macle L and Verma A; EARLY-AF Investigators. Cryoablation or drug therapy for initial treatment of atrial fibrillation. N Engl J Med 2021; 384: 305-315.

[10] Fochler F, Yamaguchi T, Kheirkahan M, Kholmovski EG, Morris AK and Marrouche NF. Late gadolinium enhancement magnetic resonance imaging guided treatment of post-atrial fibrillation ablation recurrent arrhythmia. Circ Arrhythm Electrophysiol 2019; 12: e007174.

[11] Linz D, McEvoy RD, Cowie MR, Somers VK, Nattel S, Lévy P, Kalman JM and Sanders P. Associations of obstructive sleep apnea with atrial fibrillation and continuous positive airway pressure treatment: a review. JAMA Cardiol 2018; 3: 532-540.

[12] Marulanda-Londoño E and Chaturvedi S. The interplay between obstructive sleep apnea and atrial fibrillation. Front Neurol 2017; 8: 668.

[13] Linz D, Schotten U, Neuberger HR, Böhm M and Wirth K. Negative tracheal pressure during obstructive respiratory events promotes atrial fibrillation by vagal activation. Heart Rhythm 2011; 8: 1436-1443.

[14] Miao S, Yang Y, Li R, Yin L, Zhang K, Cheng L, Xu X, Wang W, Zhao Z and Li G. The potential effects of aliskiren on atrial remodeling induced by chronic intermittent hypoxia in rats. Drug Des Devel Ther 2020; 14: 3755-3764.

[15] Hu W, Bi ZY, Chen ZL, Liu C, Li LL, Zhang F, Zhou Q, Zhu W, Song YY, Zhan BT, Zhang Q, Bi YY, Sun CC and Li DJ. Emerging landscape of circular RNAs in lung cancer. Cancer Lett 2018; 427: 18-27.

[16] Qiu LP, Wu YH, Yu XF, Tang Q, Chen L and Chen KP. The emerging role of circular RNAs in hepatocellular carcinoma. J Cancer 2018; 9: 1548-1559.

[17] Taborda MI, Ramírez S and Bernal G. Circular RNAs in colorectal cancer: possible roles in regulation of cancer cells. World J Gastrointest Oncol 2017; 9: 62-69.

[18] Hu X, Chen L, Wu S, Xu K, Jiang W, Qin M, Zhang Y and Liu X. Integrative analysis reveals key circular RNA in atrial fibrillation. Front Genet 2019; 10: 108.

[19] Zhang Y, Huang XR, Wei LH, Chung AC, Yu CM and Lan HY. miR-29b as a therapeutic agent for angiotensin II-induced cardiac fibrosis by targeting TGF-β/Smad3 signaling. Mol Ther 2014; 22: 974-985.

[20] Ma Z, Zhang K, Wang Y, Wang W, Yang Y, Liang X, Zhang Y and Li G. Doxycycline improves fibrosis-induced abnormalities in atrial conduction and vulnerability to atrial fibrillation in chronic intermittent hypoxia rats. Med Sci Monit 2020; 26: e918883.

[21] Bolger AM, Lohse M and Usadel B. Trimmomatic: a flexible trimmer for Illumina sequence data. Bioinformatics 2014; 30: 2114-2120.

[22] Glažar P, Papavasileiou P and Rajewsky N. circBase: a database for circular RNAs. RNA 2014; 20: 1666-1670.

[23] Gao Y, Wang J and Zhao F. CIRI: an efficient and unbiased algorithm for de novo circular RNA identification. Genome Biol 2015; 16: 4.

[24] Heijman J, Algalarrondo V, Voigt N, Melka J, Wehrens XH, Dobrev D and Nattel S. The value of basic research insights into atrial fibrillation mechanisms as a guide to therapeutic innovation: a critical analysis. Cardiovasc Res 2016; 109: 467-479.

[25] Sohns C and Marrouche NF. Atrial fibrillation and cardiac fibrosis. Eur Heart J 2020; 41: 1123-1131.

[26] Gal P and Marrouche NF. Magnetic resonance imaging of atrial fibrosis: redefining atrial fibrillation to a syndrome. Eur Heart J 2017; 38: 14-19.
[27] Grosman-Rimon L, Billia F, Wright E, Carasso S, Elbaz-Greener G, Kachel E, Rao V and Cherney D. Neurohormones, inflammatory mediators, and cardiovascular injury in the setting of heart failure. Heart Fail Rev 2020; 25: 685-701.
[28] Gami AS, Hodge DO, Herges RM, Olson EJ, Nykodym J, Kara T and Somers VK. Obstructive sleep apnea, obesity, and the risk of incident atrial fibrillation. J Am Coll Cardiol 2007; 49: 565-571.
[29] Gami AS, Pressman G, Caples SM, Kanagala R, Gard JJ, Davison DE, Malouf JF, Ammash NM, Friedman PA and Somers VK. Association of atrial fibrillation and obstructive sleep apnea. Circulation 2004; 110: 364-367.
[30] Ramos P, Rubies C, Torres M, Batlle M, Farre R, Brugada J, Montserrat JM, Almendros I and Mont L. Atrial fibrosis in a chronic murine model of obstructive sleep apnea: mechanisms and prevention by mesenchymal stem cells. Respir Res 2014; 15: 54.
[31] Marcus JA, Pothineni A, Marcus CZ and Bisognano JD. The role of obesity and obstructive sleep apnea in the pathogenesis and treatment of resistant hypertension. Curr Hypertens Rep 2014; 16: 411.
[32] Kang HH, Kim IK, Lee HI, Joo H, Lim JU, Lee J, Lee SH and Moon HS. Chronic intermittent hypoxia induces liver fibrosis in mice with diet-induced obesity via TLR4/MyD88/MAPK/NF-kB signaling pathways. Biochem Biophys Res Commun 2017; 490: 349-355.
[33] Braun RK, Broytman O, Braun FM, Brinkman JA, Clithero A, Modi D, Pegelow DF, Eldridge M and Teodorescu M. Chronic intermittent hypoxia worsens bleomycin-induced lung fibrosis in rats. Respir Physiol Neurobiol 2018; 256: 97-108.
[34] Wei Q, Bian Y, Yu F, Zhang Q, Zhang G, Li Y, Song S, Ren X and Tong J. Chronic intermittent hypoxia induces cardiac inflammation and dysfunction in a rat obstructive sleep apnea model. J Biomed Res 2016; 30: 490-495.
[35] Corradi D. Atrial fibrillation from the pathologist's perspective. Cardiovasc Pathol 2014; 23: 71-84.
[36] Jalife J and Kaur K. Atrial remodeling, fibrosis, and atrial fibrillation. Trends Cardiovasc Med 2015; 25: 475-484.
[37] Cardin S, Libby E, Pelletier P, Le Bouter S, Shiroshita-Takeshita A, Le Meur N, Léger J, Demolombe S, Ponton A, Glass L and Nattel S. Contrasting gene expression profiles in two canine models of atrial fibrillation. Circ Res 2007; 100: 425-433.
[38] Polyakova V, Miyagawa S, Szalay Z, Risteli J and Kostin S. Atrial extracellular matrix remodelling in patients with atrial fibrillation. J Cell Mol Med 2008; 12: 189-208.
[39] Dean RG, Balding LC, Candido R, Burns WC, Cao Z, Twigg SM and Burrell LM. Connective tissue growth factor and cardiac fibrosis after myocardial infarction. J Histochem Cytochem 2005; 53: 1245-1256.
[40] Kato T, Yamashita T, Sekiguchi A, Tsuneda T, Sagara K, Takamura M, Kaneko S, Aizawa T and Fu LT. AGEs-RAGE system mediates atrial structural remodeling in the diabetic rat. J Cardiovasc Electrophysiol 2008; 19: 415-420.
[41] Liu BC, Sun J, Chen Q, Ma KL, Ruan XZ and Phillips AO. Role of connective tissue growth factor in mediating hypertrophy of human proximal tubular cells induced by angiotensin II. Am J Nephrol 2003; 23: 429-437.
[42] Tsai CT, Tseng CD, Hwang JJ, Wu CK, Yu CC, Wang YC, Chen WP, Lai LP, Chiang FT and Lin JL. Tachycardia of atrial myocytes induces collagen expression in atrial fibroblasts through transforming growth factor β1. Cardiovasc Res 2011; 89: 805-815.
[43] Patop IL, Wüst S and Kadener S. Past, present, and future of circRNAs. EMBO J 2019; 38: e100836.
[44] Zheng Q, Bao C, Guo W, Li S, Chen J, Chen B, Luo Y, Lyu D, Li Y, Shi G, Liang L, Gu J, He X and Huang S. Circular RNA profiling reveals an abundant circHIPK3 that regulates cell growth by sponging multiple miRNAs. Nat Commun 2016; 7: 11215.
[45] Li Y, Zhang J, Huo C, Ding N, Li J, Xiao J, Lin X, Cai B, Zhang Y and Xu J. Dynamic organization of lncRNA and circular RNA regulators collectively controlled cardiac differentiation in humans. EBioMedicine 2017; 24: 137-146.
[46] Cushing L, Kuang PP, Qian J, Shao F, Wu J, Little F, Thannickal VJ, Cardoso WV and Lü J. miR-29 is a major regulator of genes associated with pulmonary fibrosis. Am J Respir Cell Mol Biol 2011; 45: 287-294.
[47] Deng Z, He Y, Yang X, Shi H, Shi A, Lu L and He L. MicroRNA-29: a crucial player in fibrotic disease. Mol Diagn Ther 2017; 21: 285-294.
[48] He Y, Huang C, Lin X and Li J. MicroRNA-29 family, a crucial therapeutic target for fibrosis diseases. Biochimie 2013; 95: 1355-1359.
[49] Li J, Cen B, Chen S and He Y. MicroRNA-29b inhibits TGF-β1-induced fibrosis via regulation of the TGF-β1/Smad pathway in primary human endometrial stromal cells. Mol Med Rep 2016; 13: 4229-4237.
[50] Wang Y, Jin BJ, Chen Q, Yan BJ and Liu ZL. MicroRNA-29b upregulation improves myocardial

fibrosis and cardiac function in myocardial infarction rats through targeting SH2B3. Eur Rev Med Pharmacol Sci 2019; 23: 10115-10122.
[51] Liang JN, Zou X, Fang XH, Xu JD, Xiao Z, Zhu JN, Li H, Yang J, Zeng N, Yuan SJ, Pan R, Fu YH, Zhang M, Luo JF, Wang S and Shan ZX. The Smad3-miR-29b/miR-29c axis mediates the protective effect of macrophage migration inhibitory factor against cardiac fibrosis. Biochim Biophys Acta Mol Basis Dis 2019; 1865: 2441-2450.
[52] Jeong JY, Kang H, Kim TH, Kim G, Heo JH, Kwon AY, Kim S, Jung SG and An HJ. MicroRNA-136 inhibits cancer stem cell activity and enhances the anti-tumor effect of paclitaxel against chemoresistant ovarian cancer cells by targeting Notch3. Cancer Lett 2017; 386: 168-178.
[53] Li J, Huang C, Zou Y, Ye J, Yu J and Gui Y. CircTLK1 promotes the proliferation and metastasis of renal cell carcinoma by sponging miR-136-5p. Mol Cancer 2020; 19: 103.
[54] Niu J, Li Z and Li F. Overexpressed microRNA-136 works as a cancer suppressor in gallbladder cancer through suppression of JNK signaling pathway via inhibition of MAP2K4. Am J Physiol Gastrointest Liver Physiol 2019; 317: G670-G681.
[55] Vonhögen IGC, El Azzouzi H, Olieslagers S, Vasilevich A, de Boer J, Tinahones FJ, da Costa Martins PA, de Windt LJ and Murri M. MiR-337-3p promotes adipocyte browning by inhibiting TWIST1. Cells 2020; 9: 1056.
[56] Wang Z, Yao L, Li Y, Hao B, Wang M, Wang J, Gu W, Zhan H, Liu G and Wu Q. MiR-337-3p inhibits its gastric tumor metastasis by targeting ARHGAP10. Mol Med Rep 2020; 21: 705-719.
[57] Zhang Z, Zhang L, Wang B, Wei R, Wang Y, Wan J, Zhang C, Zhao L, Zhu X, Zhang Y, Chu C, Guo Q, Yin X and Li X. MiR-337-3p suppresses proliferation of epithelial ovarian cancer by targeting PIK3CA and PIK3CB. Cancer Lett 2020; 469: 54-67.
[58] Wulandari E, Jusman SW, Moenadjat Y, Jusuf AA and Sadikin M. Expressions of collagen I and III in hypoxic keloid tissue. Kobe J Med Sci 2016; 62: E58-69.
[59] Liu Y, Xu B, Wu N, Xiang Y, Wu L, Zhang M, Wang J, Chen X, Li Y and Zhong L. Association of MMPs and TIMPs with the occurrence of atrial fibrillation: a systematic review and meta-analysis. Can J Cardiol 2016; 32: 803-813.
[60] Shinde AV, Humeres C and Frangogiannis NG. The role of α-smooth muscle actin in fibroblast-mediated matrix contraction and remodeling. Biochim Biophys Acta Mol Basis Dis 2017; 1863: 298-309.
[61] Su H, Su H, Liu CH, Hu HJ, Zhao JB, Zou T and Tang YX. H(2)S inhibits atrial fibrillation-induced atrial fibrosis through miR-133a/CTGF axis. Cytokine 2021; 146: 155557.
[62] Zhao Z, Li R, Wang X, Li J, Xu X, Liu T, Liu E and Li G. Suppression of experimental atrial fibrillation in a canine model of rapid atrial pacing by the phosphodiesterase 3 inhibitor cilostazol. J Electrocardiol 2020; 60: 151-158.

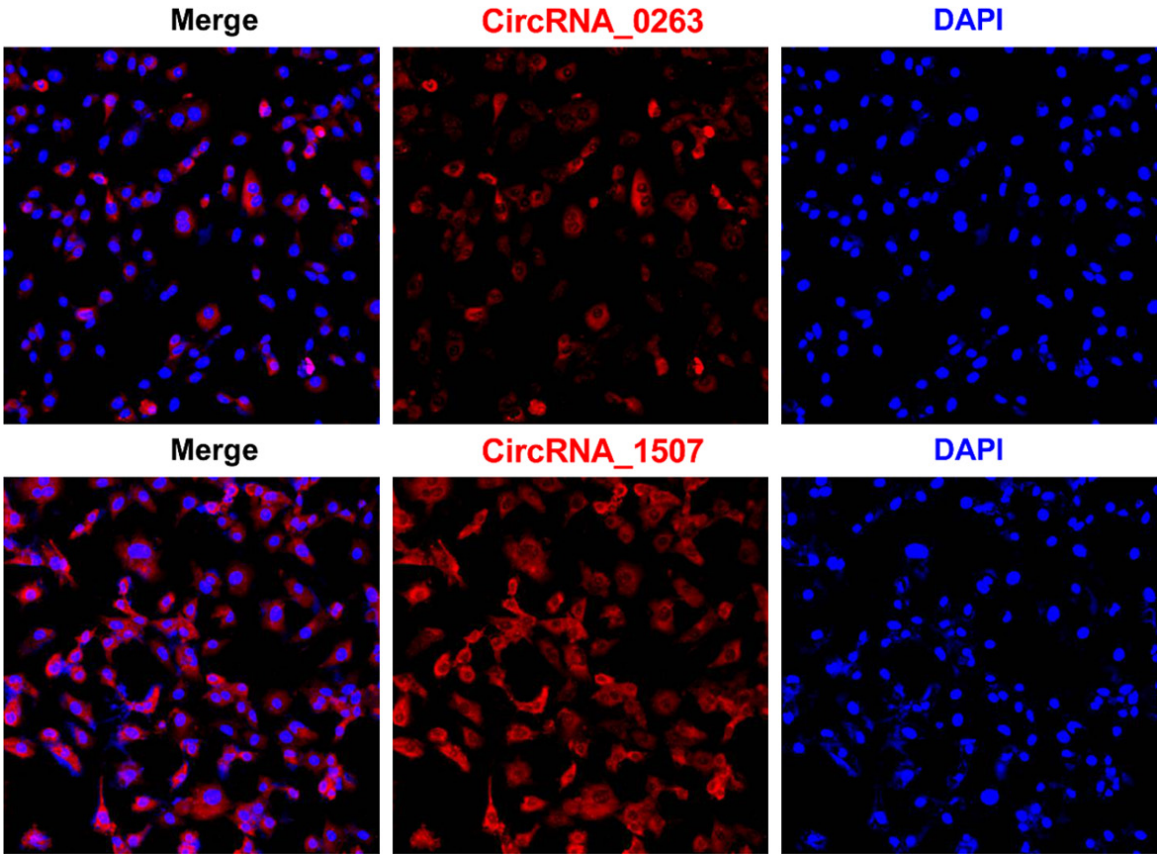

Figure S1. Rat atrial fibroblasts were stained with circRNA_0263 or circRNA_1507 probe (red) and a nuclear marker [DAPI (4',6-diamidino-2-phenylindole), blue], and imaged under confocal microscopy.

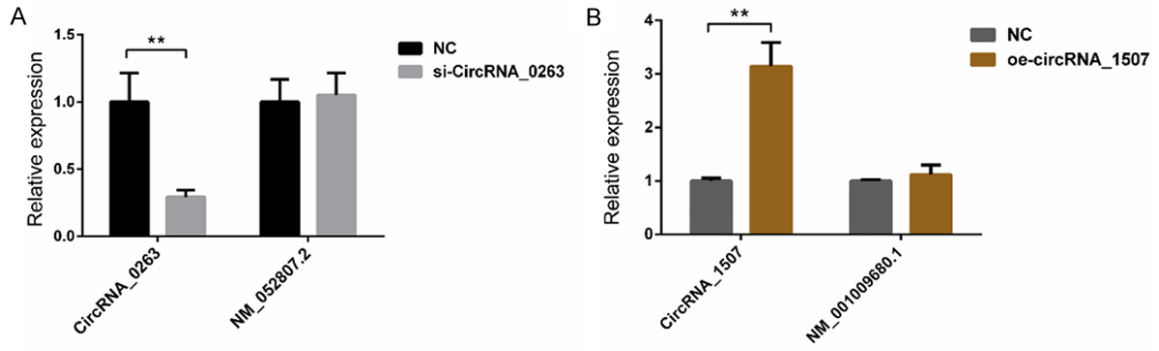

Figure S2. The effect of knocking down of circRNA_0263 and overexpressing of circRNA_1507 on homologous mRNA was detected by quantitative real-time polymerase chain reaction (qRT-PCR). **, $P < 0.01$.